J Appl Electrochem (2009) 39:719–725
DOI 10.1007/s10800-008-9715-z

ORIGINAL PAPER

Effects of anodization and electrodeposition conditions on the growth of copper and cobalt nanostructures in aluminum oxide films

Abbas Ghaddar · Jacek Gieraltowski · Frederic Gloaguen

Received: 11 June 2008 / Accepted: 5 November 2008 / Published online: 21 November 2008

Abstract Anodic aluminum oxide (AAO) films were prepared by alternative current (ac) oxidation in sulfuric acid and phosphoric acid solution. The porous structure of the AAO templates was probed by ac electrodeposition of copper. AAO templates grown using an applied square waveform signal in cold sulfuric acid solution exhibit a greater pore density and a more homogeneous barrier layer. UV–vis–NIR reflectance spectra of the Cu/AAO assemblies exhibit a plasmon absorption peak centered at 580 nm, consistent with the formation of Cu nanostructures slightly larger than 10 nm in diameter. Spectroscopic data also indicate that there is little or no oxide layer surrounding the Cu nanostructures grown by ac electrodeposition. The effect of pH of the cobalt plating solution on the magnetic properties of the Co/AAO assemblies was also investigated. Co nanowire arrays electrodeposited at pH 5.5 in H_2SO_4-grown AAO templates exhibit a fair coercivity of 1325 Oe, a magnetization squarness of about 72%, and a significant effective anisotropy.

Keywords Aluminum · Anodization · Cobalt · Copper · Electrodeposition · Nanowire

Electronic supplementary material The online version of this article (doi:10.1007/s10800-008-9715-z) contains supplementary material, which is available to authorized users.

A. Ghaddar · J. Gieraltowski
Laboratoire de Magnétisme de Bretagne, FRE CNRS 2697, Université de Bretagne Occidentale, CS 93837, 29238 Brest Cedex, France

F. Gloaguen (✉)
Laboratoire de Chimie Electrochimie Moléculaires et Chimie Analytique, UMR CNRS 6521, Université de Bretagne Occidentale, CS 93837, 29238 Brest Cedex, France
e-mail: fgloague@univ-brest.fr

1 Introduction

Metal nanostructures continue to attract considerable attention because of their size- and shape-dependent catalytic, electronic, optical, and magnetic properties [1, 2]. Colloidal solutions and nanoparticles/oxide composites of copper, silver and gold, have an unusual optical absorption in the visible region of the spectrum due to the surface-plasmon resonance [3–6]. Nanowires of ferromagnetic metal, such as Fe, Ni and Co, exhibit hysteresis loop with improved coercivity and squareness, as compared to thin film or bulk material [7]. Among the different synthetic methods described in the literature, template-directed electrodeposition remains one of the easiest approaches to control the geometry of the nanostructures [8, 9]. For example, nanowires with a high aspect ratio can be readily prepared by electrochemical reduction of metal ions within the pores of commercially available membranes with one side covered by a conducting layer [10–12]. Anodic aluminum oxide (AAO) template is another widespread pathway to diverse metal nanostructures [5, 13]. A porous oxide layer is formed upon oxidation of aluminum. The pore diameter, the pore density, and the pore depth depend on the applied potential, temperature, and electrolyte [14]. Masuda et al. [15] reported that a two-step anodization process in acid electrolyte gives under carefully controlled experimental conditions a close-packed array of pores normal to the substrate. In the course of aluminum oxidation, a barrier layer is formed at the bottom of the pores [16, 17]. This barrier layer hinders the electrochemical reduction of the metal ions under direct current (dc) electrolysis conditions. In order to grow metal nanostructures into AAO template, it is necessary either to separate the porous oxide layer from the remaining aluminum substrate [18], or to decrease the thickness of the barrier layer by

chemical or electrochemical etching [19, 20]. The implementation of these two strategies is, however, complex and time consuming. For applications in catalysis, where metal nanoparticule/support interaction is an important parameter, or the fabrication of lab-on-chip devices, it might be interesting to develop a rapid and simple method for preparing arrays of metal nanostructures into 'as prepared' AAO templates. Under alternative current (ac) electrolysis conditions, the barrier layer between the aluminum substrate and the electrolyte is preferentially conductive during the cathodic half-cycle. This rectifying property allows for the reduction of the metal ions in the pore while decreasing the oxidation rate of the deposited metal [21]. A number of metals were successfully electrodeposited by ac electrolysis in AAO layers [11]. However, as compared to dc electrodeposition into a porous membrane, ac electrodeposition through the barrier layer provides a less easy control over the amount and the composition of deposited metal. The effects of several ac electrodeposition parameters on the filling of the AAO template by Ag and Cu nanowires were recently investigated in detail [22, 23]. Whereas anodization of the aluminum foil was in most cases carried out at a constant potential exceeding 40 V, Kawai and Ueda carried out aluminum anodization under ac conditions at ±15 V [24]. Cobalt and nickel electrodeposited in the resulting aluminum oxide film form columnar nanostructures with a remarkable magnetic anisotropy. Ac oxidation of aluminum appears thus as an alternative approach for the fabrication of AAO templates. The thickness of the barrier layer at the bottom of the pores is proportional to the applied anodization potential (about 1 nm V^{-1}). Ac anodization carried out at a lower potential than dc anodization might thus lead to AAO template with a thinner barrier layer, and hence to a more homogeneous filling of the pore.

In the present paper we report the fabrication of AAO templates by a single step anodization under ac conditions in sulfuric acid or phosphoric acid. The effects of the anodizing conditions on the AAO structure were probed by copper electrodeposition and UV–vis–NIR spectroscopy of the resulting Cu/AAO composite layer. Preliminary results on the magnetic properties of Co nanowire arrays grown by electrodeposition at different pH are also reported.

2 Experimental

The glassware and the platinum auxiliary electrode were cleaned with *aqua regia*. The solutions were prepared from analytical-grade chemicals and deionized water (MilliQ, Millipore). For anodization and electrodeposition experiments, the ac signal (±15 V, 50 Hz, sine or square waveform) applied to the aluminum foil and the platinum auxiliary electrode was generated using a HP 3311A function generator coupled with a HP 6823A power supply—amplifier. The current against time responses were recorded using a digital multimeter (Pierron IS5000). Anodic oxide layers were grown on commercially available Al foils (Roth). The foils were degreased in acetone for 15 min using an ultrasonic bath, electropolished to a mirror-like finish at +8 V for 2 min in a mixture of $HClO_4$ (70% wt) and EtOH in a 1/4 vol. ratio, immersed for 2 min in a hot Na_2CO_3 solution (25 g L^{-1}, 0.24 M) to remove the native oxide layer, briefly etched in a concentrated HNO_3 solution (10% vol., 1.4 M), and then rinsed with deionized water. Adhesive tape was used to separate the immersed part of the aluminum foil from the electrical contact area to prevent runaway oxidation at the electrolyte/air/aluminum interface. Anodization was carried out under strong magnetic stirring in either H_2SO_4 (10% vol., 1.8 M) at 1 °C or H_3PO_4 (10% vol., 1.5 M) at 35 °C. Prior to electrodeposition, the back and the edges of the anodized aluminum foil were covered with adhesive tape to produce an electrode with only one face exposed, and the electrode was then soaked in water for at least 15 min. Copper and cobalt plating electrolytes were prepared by, respectively, dissolving $CuSO_4$,$5H_5O$ (50 g L^{-1}, 0.20 M) or $CoSO_4$,$7H_2O$ (121 g L^{-1}, 0.43 M) along with H_3BO_3 (30 g L^{-1}, 0.48 M) in deionized water. Electrodeposition was conducted at room temperature with no stirring. UV–vis–NIR reflectance spectra of carefully dried AAO samples were recorded using a JASCO V-670 spectrophotometer equipped with a 60 mm integrating sphere. The magnetic properties of Co nanowire arrays were studied by vibrating sample magnetometer (VSM) measurements at room temperature. The hysteresis loops were recorded for an applied magnetic field parallel and normal to the AAO template surface.

3 Results and discussion

3.1 Anodization

Ac anodization was performed at 1 °C in sulfuric acid solution and at 35 °C in phosphoric acid solution, the former acid being the most corrosive. With both acids, strong gas evolution was observed in the course of anodization. The ac current was recorded each second and the resulting current against time plots are shown in Fig. 1. After an initial current decay, the current reaches a limiting value at $t > 30$ s ($\approx$1,500 cycles). This indicates a steady state situation in which the rate of anodic layer formation equals the rate of chemical dissolution. The limiting current density is about 1/3 time larger with an applied square waveform signal, but does not significantly depend on the nature of the electrolyte (H_2SO_4 or H_3PO_4) (Fig. 1). When

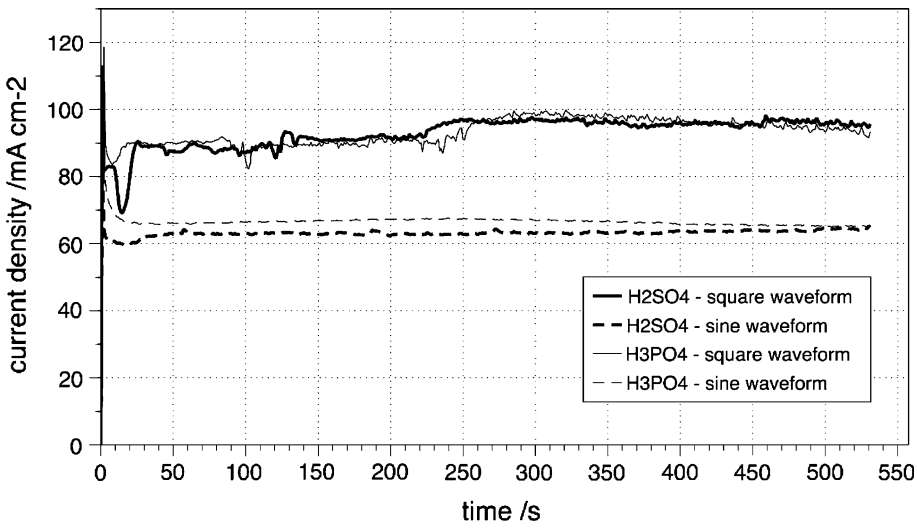

Fig. 1 Current against time responses recorded each second for aluminum foils anodized at ±15 V (50 Hz) in either 1.8 M H_2SO_4 at 1 °C or 1.5 M H_3PO_4 at 35 °C

a square waveform signal was applied, there is a sharp falling and rising of the current at the short anodization times ($t < 20$ s). This feature is less pronounced with a sine waveform signal in sulfuric acid solution, and barely observed in phosphoric acid solution. The current falling and rising might be ascribed to the nucleation and growth of the pores on the barrier layer. These observations suggest hence that anodization in sulfuric acid with an applied square waveform signal generates the largest pore density in the AAO layer.

UV–visible–NIR reflectance spectra of the anodized aluminum foils exhibit all an absorption peak at about 820 nm (Fig. 2). We recorded a very similar spectrum for an aluminum foil anodized at +50 V (dc) during 20 min in phosphoric acid at 35 °C (not shown). This indicates that the anodization conditions have little effects on the UV–visible–NIR responses collected in reflectance mode. However, for an AAO template grown at +50 V (dc) in oxalic acid and then separated from the aluminum substrate, the spectrum collected in transmission mode does not exhibit any absorption peaks in the 400–1,800 nm range [5]. The absorption at about 820 nm may thus be ascribed to the presence of a barrier layer at the bottom of the pores and/or to the utilization of an integration sphere to collect the spectra.

3.2 Electrodeposition

3.2.1 Copper electrodeposition

Copper is easily electrodeposited at a low overpotential, which makes the Cu^{2+}/Cu^0 couple a suitable probe for investigating electrodeposition in the AAO templates. In the present work, pore filling was achieved by ac electrolysis of a 0.2 M $CuSO_4$ + 0.45 M H_3BO_3 solution (pH ≈ 3.5). H_3BO_3 acts as a buffer that avoids corrosive attack of the AAO template and limits the hydrogen evolution. We observed first that no copper electrodeposition

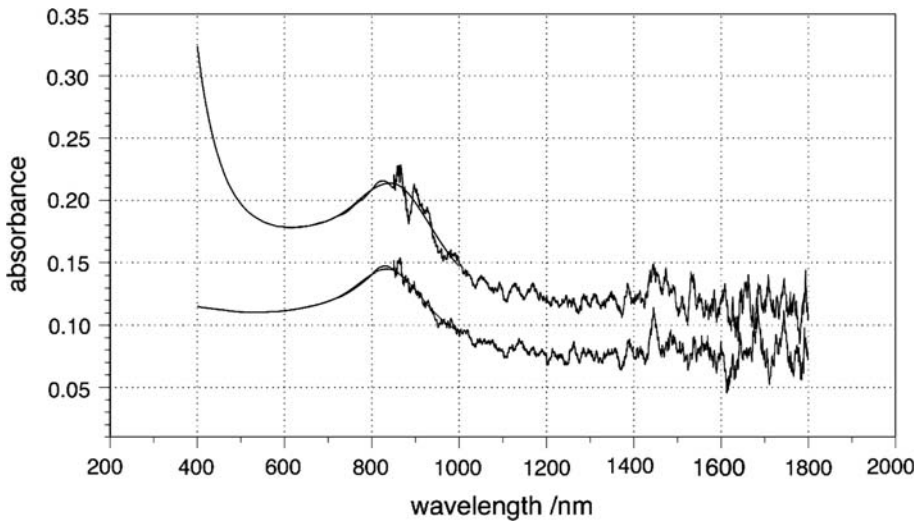

Fig. 2 UV–visible–NIR reflectance spectra of aluminum foils anodized at ±15 V (50 Hz, square waveform). Top: 1.8 M H_2SO_4, 1 °C, 10 min. Bottom: 1.5 M H_3PO_4, 35 °C, 20 min

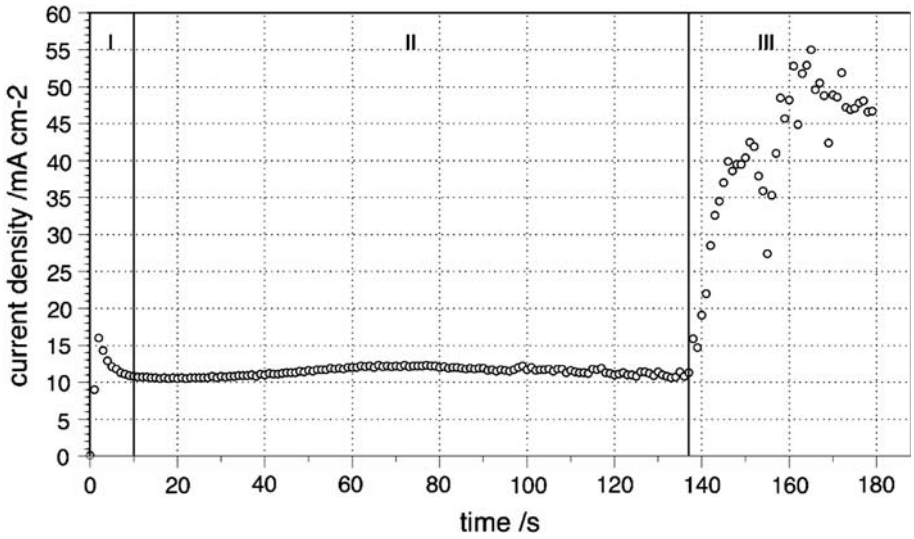

Fig. 3 Current against time response for Cu electrodeposition in H_2SO_4-grown AAO template. Electrodeposition at ±15 V (50 Hz, square waveform) in 0.2 M $CuSO_4$ + 0.48 M H_3BO_3 (pH 3.5)

occurs for an applied potential of ±5 V, suggesting that the insulating properties of the barrier layer are similar to those encountered with AAO templates grown under dc conditions. The quality of the AAO template was determined by visual inspection of the Cu deposit after an electrolysis period of 5 min at ±15 V (50 Hz). In the case of AAO templates obtained by using a sine waveform signal, Cu deposit was either not observed for H_3PO_4-grown AAO template or very heterogeneous for H_2SO_4-grown AAO template. In the case of AAO templates obtained by using a square waveform signal, the color of the aluminum foil turns rapidly green, consistent with the deposition of Cu nanoparticles (see below). At longer electrolysis time, we observed the formation of a bulk copper layer partly covering the aluminum surface. These observations support the conclusions derived from the current against time responses recorded in the course of the anodization process (Fig. 1), and indicate that a square waveform signal gives the best AAO templates.

The pore filling process was followed by recording the current response in the course of electrodeposition. The resulting current against time plot can be divided into three regions (Fig. 3). There is first a rapid rise and fall of the reduction current (region I), which can be ascribed to a nucleation and growth process at the bottom of the pores. The current reaches then a plateau value (region II) corresponding to the filling of the pores by Cu. At longer deposition time, the current increases sharply and/or exhibits some noise (region III) because of the complete filling of most of the pores and the growth of a Cu layer on top of the AAO template. Although the current response most certainly includes additional contributions due to hydrogen evolution and oxidation/reduction of aluminum, the current against time plot allows for an easy control of the filling process of the AAO template.

The pores are completely filled by copper after a period of about 140 s in the case of H_2SO_4-grown AAO template (10 min anodization at 1 °C) and about 110 s in the case of the H_3PO_4-grown AAO template (20 min anodization at 35 °C). A commercially ion-track etched polycarbonate membrane (thickness: 6 μm, pore diameter: 15 nm) was used as template for comparison. The current against time response is very similar to that recorded in the case of the H_3PO_4-grown AAO template (see Fig. 4 and Fig. S1 in electronic supplementary material). The filling of the pores of the 6 μm-thick polycarbonate membrane takes about 180 s. Assuming a pore-filling rate of the same order of magnitude in polycarbonate and AAO templates, this suggests that the thickness of the AAO templates prepared by ac anodization is of the order of magnitude of several micrometers. This result is in agreement with previously reported work [24].

For H_2SO_4-grown AAO template, the current in the region II is very stable indicating that most of the pores are filled at the same rate (Fig. 3). In contrast, for H_3PO_4-grown AAO template, the current in region II is noisy and exhibits many spikes indicating that some pores are filled more rapidly than others (Fig. 4). The decrease of the $Cu(SO)_4$ concentration from 0.2 to 0.02 M in the plating electrolyte leads to a more stable deposition current in the region II. These observations strongly suggest that the pore filling in H_2SO_4-grown AAO template is more homogeneous than in H_3PO_4-grown AAO template. Since the thickness of the H_3PO_4-grown AAO template is not smaller than that of the H_2SO_4-grown AAO template (see above), this discrepancy is to be ascribed to the chemistry and/or the structure of the barrier layer. The concentration of acid ions incorporated in the barrier layer depends on acid used for anodization. For AAO template grown under dc conditions, the sulfate concentration in the barrier layer is

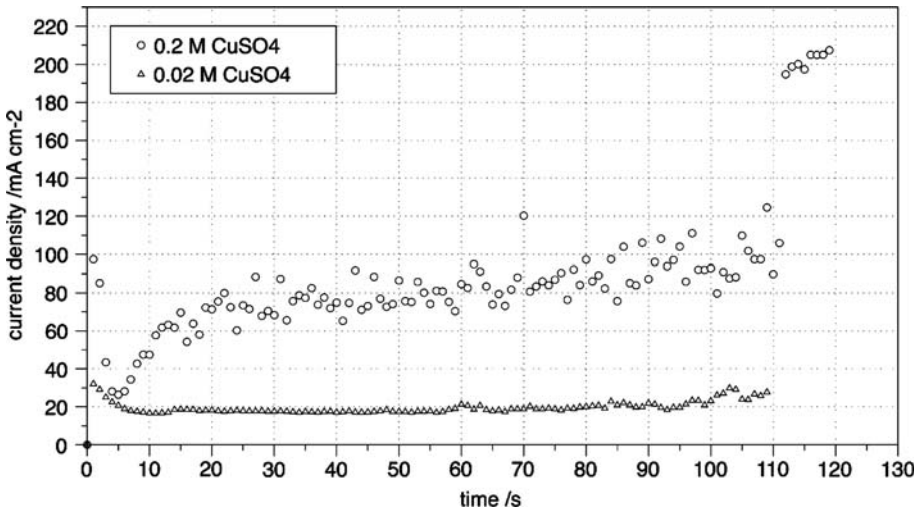

Fig. 4 Current against time responses for Cu electrodeposition in H_3PO_4-grown AAO template. Electrodeposition at ±15 V (50 Hz, square waveform) in x M $CuSO_4$ + 0.48 M H_3BO_3 (x = 0.2, 0.02, pH 3.5)

12–14%wt, whereas the oxalate concentration is only 2–4%wt [17]. A similarly low acid ion concentration may be anticipated in the case of H_3PO_4-grown AAO template. In addition, it is very likely that a barrier layer at the bottom of the pores grown during 10 min in cold sulfuric acid solution contains less defects than a barrier layer at the bottom of the pores grown during 20 min in warm phosphoric acid solution. The Cu electrodeposition current is larger for H_3PO_4-grown AAO template (Figs. 3, 4), but this might also be due to the larger diameter of the pores.

UV–visible–NIR reflectance spectra of Cu/AAO composites obtained by electrolysis of a 0.20 M $CuSO_4$ + 0.48 M H_3BO_3 solution during a period of 60 s, i.e. before complete filling, are presented in Fig. 5. There is an absorption peak near 580 nm in the case of the H_2SO_4-grown AAO template and at about 590 nm in the case of the H_3PO_3-AAO template. These peaks are assigned to the plasmon absorption of the copper nanostructures embedded in the AAO templates. Generally, the maximum of the plasmon absorption is red-shifted with increasing nanoparticule diameters; however, its position depends also, among other parameters, on the shape (i.e. the aspect ratio) of the nanoparticles [25, 26]. For 10 nm-diameter copper particles formed in reverse micelles, the maximum of the plasmon absorption is located at 570 nm [3]. The red-shift observed for the Cu/AAO composites may be explained by a slightly larger diameter and/or the rod-like shape of the Cu nanostructures. No absorption was observed around 800 nm [3], which indicates that there is little or no oxide layer surrounding the Cu nanostructures grown by ac electrodeposition. This emphasizes the rectifying properties of the barrier layer.

3.2.2 *Cobalt electrodeposition*

Ferromagnetic nanowires electrodeposited in a porous template represent a model system for studying array of uniaxial nanomagnets. The effective magnetic anisotropy of a nanowire array results from the competition between several effects: the interaction between nanowires, the shape

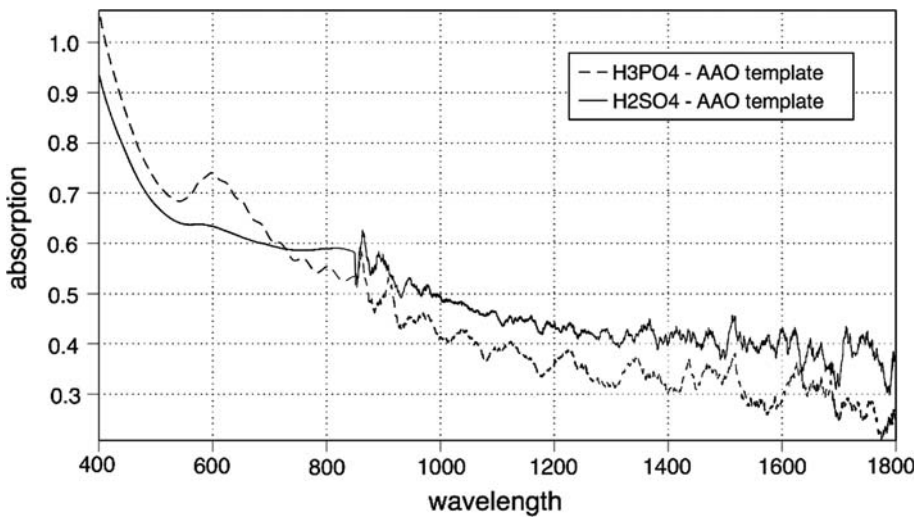

Fig. 5 UV–vis–NIR reflectance spectra of Cu/AAO template composite layers. Electrodeposition at ±15 V (50 Hz, square waveform) for 1 min in 0.2 M $CuSO_4$ + 0.48 M H_3BO_3 (pH 3.5)

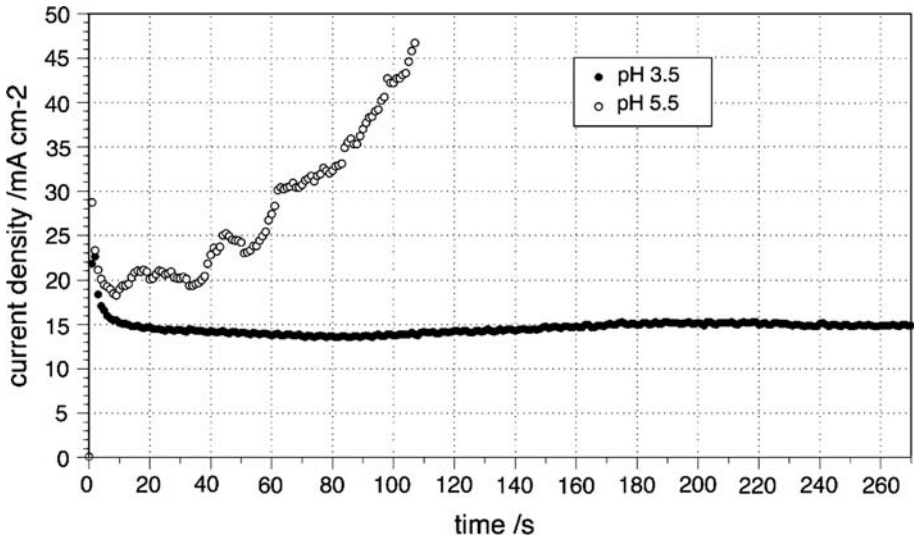

Fig. 6 Current against time response for Co electrodeposition in H_2SO_4-grown AAO template. Electrodeposition conditions: 0.43 M $CoSO_4$ + 0.48 M H_3BO_3 (pH 3.5 or 5.5), ±15 V, 50 Hz, square waveform; pH was increased by addition of NaOH

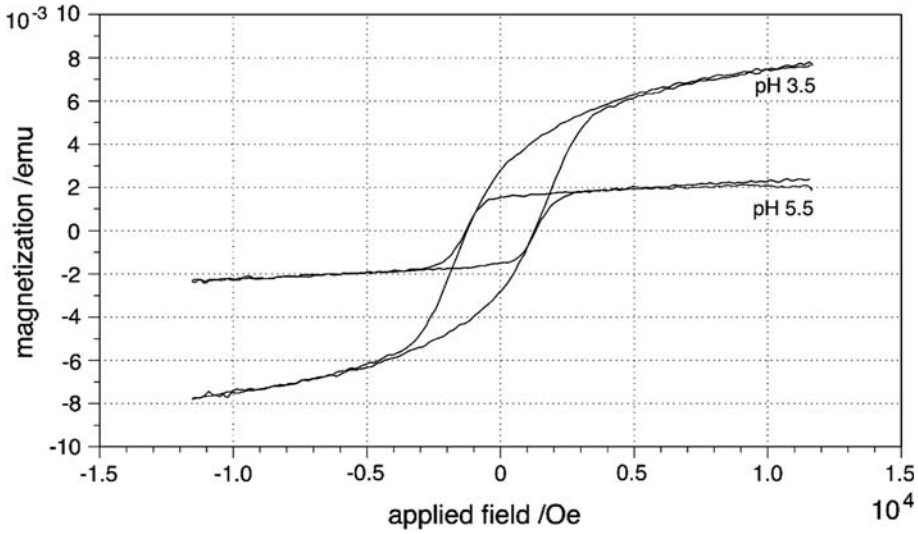

Fig. 7 Magnetization curves for Co nanowires embedded in H_2SO_4-grown AAO template with the applied magnetic field normal to the AAO surface. Ac electrodeposition at ±15 V (50 Hz, square waveform) for 5 min (pH 3.5) and 1 min (pH 5.5), respectively

anisotropy of individual nanowires, and an average magnetocrystalline anisotropy [7]. It is well known that the crystallographic structure of the Co electrodeposits is affected by the pH of the plating solution [27]. In the present work, Co nanowire arrays were deposited at pH 3.5 and 5.5 by ac electrolysis in H_2SO_4-grown AAO templates. The current against time responses recorded in the course of Co electrodeposition are shown in Fig. 6. At pH 3.5, the deposition current is stable and we did not observe the feature characteristic of a complete pore filling (i.e. analogous to region III in Fig. 3), even after a deposition period of 10 min. In contrast at pH 5.5, the deposition current is more noisy and the current against time response suggests that some of the pore a completely filled after a deposition period of about 40–60 s. On the other hand, the magnetization at saturation M_s, which is proportional to the amount of deposited Co, is larger after electrolysis during 5 min at pH 3.5 than after electrolysis during 1 min at pH 5.5 (Fig. 7). We don't have at present any clear explanations for these results. For an applied field normal to AAO surface, the arrays of Co nanowires prepared at pH 3.5 and pH 5.5 exhibit a very similar coercivity value of $H_c(\perp) = 1220$ and 1325 Oe, respectively. These values are slightly larger than those previously recorded for Co/AAO assemblies in which the pore diameter is about 10 nm and the interpore spacing is about 40 nm [24]. As the coercivity usually increases as the diameter of the ferromagnetic nanowire decreases, we postulate that the pore diameter in the H_2SO_4-grown AAO template is not larger than 10 nm. However, higher coercivity values (i.e. $H_c(\perp) = 1600 - 1800$ Oe) were reported for 50 nm-diameter Co nanowire arrays in which the interpore spacing was 100 nm, emphasizing of the effect of the nanowire interactions on H_c [28]. The crystalline structure of Co nanowires greatly depends on the pH of the plating solution, which, in turn, has an effect on the magnetocrystalline anisotropy [27]. Increasing the plating solution pH

from 3.5 to 5.5 leads to a significant increase in the remanent magnetization $M_r(\perp)$ from 38 to 72% of the saturated magnetization M_s recorded for an applied field normal to the AAO template surface (Fig. 7). This result shows that at pH 5.5, the electrochemical growth of the nanowires takes place with a preferred crystalline orientation of the Co hexagonal close-packed *c*-axis parallel to the nanopore axis, improving the overall magnetic anisotropy of the system (see Table S1 in electronic supplementary material).

4 Conclusion

Cu electrodeposition experiments indicate that AAO templates grown using an applied square waveform signal in cold sulfuric acid solution exhibit a greater pore density and a more homogeneous barrier layer than those grown in warm phosphoric acid solution and/or using an applied sine waveform signal. As a result, ac electrodeposition at pH 5.5 of Co in H_2SO_4-grown AAO templates leads to nanowire arrays with fair coercivity, good magnetization squareness and significant anisotropy. The effects of composition and pH of the plating electrolyte on the magnetic properties of Co/AAO and CoNi/AAO assemblies are currently under investigation in our laboratory.

The ease of fabrication of Co nanowire arrays reported in this work combined with the possibility of controlling the effective magnetic anisotropy opens the way to various applications and, in particular, cobalt-based multilayered giant magnetoresistive sensing [29].

References

1. Murphy CJ (2002) Science 298:2139
2. Mirkin CA (2005) Small 1:14
3. Lisiecki I, Pileni M (1993) J Am Chem Soc 115:3887
4. Preston CK, Moskovoits M (1993) J Phys Chem 97:8495
5. Foss CA, Hornyak GL, Stockert JA, Martin CR (1994) J Phys Chem 98:2963
6. Link S, El-Sayed M (1999) J Phys Chem B 103:4212
7. Sun L, Hao Y, Chien C-L, Searson PC (2005) IBM J Res & Dev 49:79
8. Penner RM, Martin CR (1987) Anal Chem 59:2625
9. Menke EJ, Thompson MA, Xiang C, Yang LC, Penner RM (2006) Nature Mater 5:914
10. Doudin B, Wegrowe JE, Gilbert SE, Scarani V, Kelly D, Meier JP, Ansermet J-P (1998) IEEE Trans Magn 34:968
11. He H, Tao NJ (2003) In: Nalwa HS (ed) Encyclopedia of nanosciences and nanotechnology, vol X. American Scientific Publishers, New York, p 1
12. Bentley AK, Farhoud M, Elllis AB, Lisensky GC, Nickel A-ML, Crone WC (2005) J Chem Educ 82:765
13. Piao Y, Lim H, Chang JY, Lee W-Y, Kim H (2005) Electrochim Acta 50:2997
14. Keller F, Hunter MS, Robinson DL (1953) J Electrochem Soc 100:411
15. Masuda H, Fukuda K (1995) Science 268:1466
16. Gruberger J, Gileadi E (1986) Electrochim Acta 31:1531
17. Vrublevsky I, Parkoun V, Sokol V, Schreckenbach J (2004) Appl Surf Sci 236:270
18. Hulteen JC, Martin CR (1997) J Mater Chem 7:1075
19. Choi J, Sauer G, Nielsch K, Wehrspohn RB, Gosele U (2003) Chem Matter 15:776
20. Ohgai T, Hoffer X, Gravier L, Ansermet J-P (2004) J Appl Electrochem 34:1007
21. Nielsch K, Müller F, Li A-P, Gösele U (2000) Adv Mater 12:582
22. Sauer G, Brehm G, Schneider S, Nielsch K, Wehrspohn RB, Choi J, Hofmeister H, Gösele U (2002) J Appl Phys 91:3243
23. Gerein NJ, Haber JA (2005) J Phys Chem B 109:17372
24. Kawai S, Ueda R (1975) J Electrochem Soc 122:32
25. Jana NR, Gearheart L, Murphy CJ (2001) Adv Mater 13:1389
26. Duan J-L, Liu J, Yao H-J, Mo D, Hou M-D, Sun Y-M, Chen Y-F, Zhang L (2008) Mater Sci Eng B 147:57
27. Darques M, Encinas A, Vila L, Piraux L (2004) J Phys D Appl Phys 37:1411
28. Pan H et al (2005) J Phys Chem B 109:3094
29. Darques M, Bogaert AS, Elhoussine F, Michotte S, Medina JT, Encinas A, Piraux L (2006) J Phys D Appl Phys 39:5025